

## SYNERGY BETWEEN OPTICAL (GAIA) AND RADIO (VLBI) ASTROMETRIC RESEARCHES

N. Sakai<sup>1</sup>

### RESUMEN

La astrometría óptica y en radio se han convertido en herramientas fundamentales para el mapeo de la Vía Láctea. En este trabajo damos un ejemplo de la sinergia entre la astrometría en radio y óptico, en el estudio de los brazos espirales de nuestra galaxia. La distribución espacial y la cinemática de las estrellas y el gas, nos indican una nueva y compleja imagen de dichos brazos. La sinergia de los estudios astrométricos a diferentes longitudes de onda se verá incrementada con los futuros proyectos astrométricos en el infrarrojo (e.g. Jasmine; *Gaia* NIR) previstos para los años 2020-2030s.

### ABSTRACT

Optical and radio astrometry have become significant for mapping the Milky Way. We introduce an example of synergy between optical and radio astrometry on a research of the Galactic spiral arms. Kinematics and spatial distribution of star and gas indicate a new and complex picture of the Galactic spiral arms. Synergy of astrometric study at multi-wavelength would be enhanced thanks to future infrared astrometric projects (e.g., Small Jasmine; *Gaia*NIR) in 2020-2030s.

*Key Words:* astrometry — Galaxy: disc — Galaxy: kinematics and dynamics — parallaxes — proper motions

### 1. INTRODUCTION

Astrometry combined with spectroscopy allows us to obtain 6-d phase information of astronomical objects (i.e. 3-dimensional position and motion). Optical astrometric results of *Gaia* DR2 containing more than 1.3 billion parallaxes with uncertainties larger than 20 microarcsecond ( $\mu$ as) were published in 2018 (Gaia Collaboration et al. 2018). The number of citations for Gaia Collaboration et al. (2018) is  $\sim 2,500$  as of February, 2020.

VLBI astrometry at radio wavelength has succeeded to measure the smallest parallax ever reported (i.e.  $0.049 \pm 0.006$  mas; Sanna et al. 2017), and it enables one to map the whole structure of the Milky Way. Combining optical astrometric results with radio (VLBI) astrometric ones can delineate the structure of the Milky Way such as the spiral arm, bars, warp, halo and so on.

Here, we introduce a synergy between optical and radio astrometry on the spiral-arm research of the Milky Way.

### 2. ASTROMETRY OF THE SPIRAL ARM

Theories of the spiral arm are well summarized in Dobbs & Baba (2014) and references therein. To validate each theory, comparing kinematics and spatial

distribution between star and gas is important and it can be conducted with *Gaia* and VLBI astrometric results.

We introduce an example of the comparison study on kinematics (Sakai et al. 2019) and spatial distribution (Miyachi et al. 2019) of the Galactic spiral arms in the following sections.

#### 2.1. Kinematics

Sakai et al. (2019) examined non-circular motion of the Perseus spiral arm as shown in Figures 1 and 2. These indicate that gas kinematics around the Perseus arm could be explained by a Galactic shock model (Roberts 1972). However, they revealed that gas kinematics of the Local and Sagittarius arms could not be explained by the same model.

Using *Gaia* DR2, Sakai et al. (2019) reported that stellar kinematics of the Local and Sagittarius arms is not consistent with the Galactic shock model. Regarding the stellar kinematics of the Perseus arm, they could not obtain enough sample due to a systematic parallax error of 0.1 mas as reported by Lindgren et al. (2018) (please also see Figure 2 of Xu et al. 2018).

#### 2.2. Spatial Distribution

Using cross-matched data of *Gaia* DR2 and 2MASS Point Source Catalog, Miyachi et al. (2019) found an arm-like stellar overdensity of 1 Gyr age

<sup>1</sup>Korea Astronomy and Space Science Institute  
Daedeokdae-ro 776, Yuseong-gu Daejeon 34055, Republic of Korea (nsakai@kasi.re.kr).

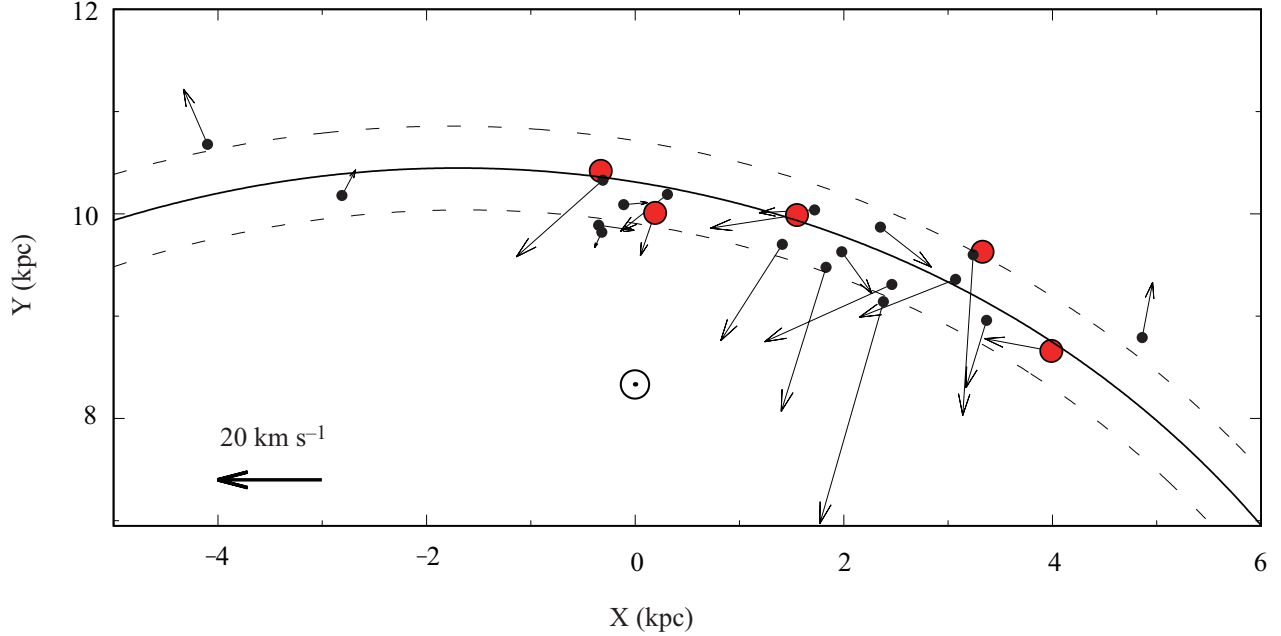


Fig. 1. Spatial distribution and non-circular motions of Perseus-arm sources, taken from Sakai et al. (2019). Large red and small black filled circles show new and previous VLBI astrometric results. For clarity, only sources whose motion uncertainties are less than  $20 \text{ km s}^{-1}$  are plotted. A scale of  $20 \text{ km s}^{-1}$  (thick arrow) is displayed at the lower left. The solid curve represents a fitted logarithmic spiral model and the dashed lines indicate  $\pm 1\sigma$  width. The Sun is at  $(X, Y) = (0, 8.34)$  kpc. The non-circular motions are with respect to Galactic constants ( $R_0 = 8.34$  kpc and  $\Theta_0 = 241 \text{ km s}^{-1}$ ) and a solar motion of  $(U_\odot, V_\odot, W_\odot) = (10.5, 14.4, 8.9) \text{ km s}^{-1}$  (Reid et al. 2014).

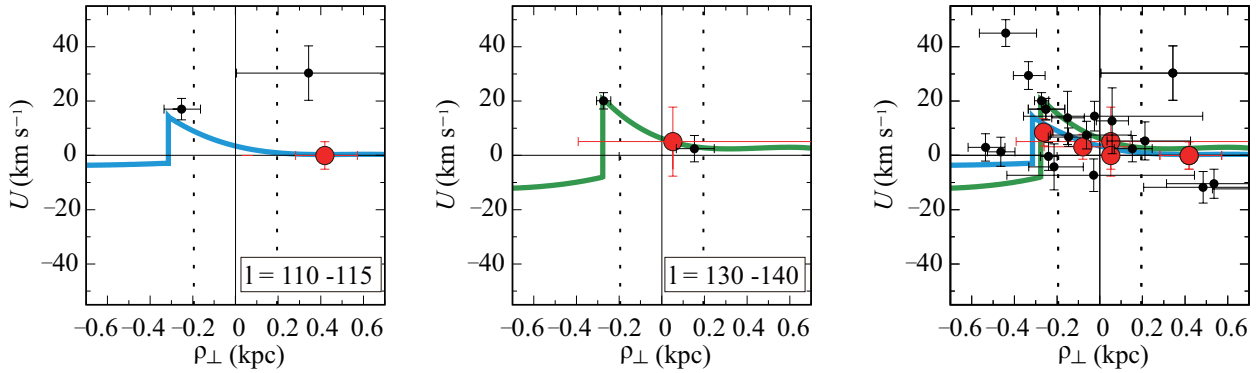


Fig. 2. Sakai et al. (2019): (*Left*) Non-circular motion toward the Galactic center ( $U$ ) is expressed as a function of distance perpendicular to the Perseus arm ( $\rho_\perp$ ) for masers in the Galactic longitude range  $l = 110\text{--}115$  deg. Large red and small black circles show new and previous VLBI astrometric results, respectively. The cyan curve represents a hydrodynamic-shock model with a spiral pitch angle of 12 degrees, a pattern speed of  $12.5 \text{ km s}^{-1} \text{ kpc}^{-1}$ , a gas dispersion speed of  $8 \text{ km s}^{-1}$  and a spiral potential with a 7.5% enhancement compared to the axisymmetric potential (taken from Figure 4 of Roberts 1972). (*Middle*) Same as (*left*) but for sources at the Galactic longitude range  $l = 130\text{--}140$  deg. A hydrodynamic shock model shown by a green curve is from Figure 3 of Roberts (1972). (*Right*) Same as (*left*) but for VLBI astrometric results from the entire Perseus arm. The cyan and green curves from the other panels are superimposed.

stars in the solar neighborhood as shown in Figure 3. The stellar overdensity is well followed by  $\text{H II}$  regions (open blue squares in Figure 3), and is slightly devi-

ated with a larger pitch angle from the Local spiral arm traced with high-mass star forming regions (i.e. gas).

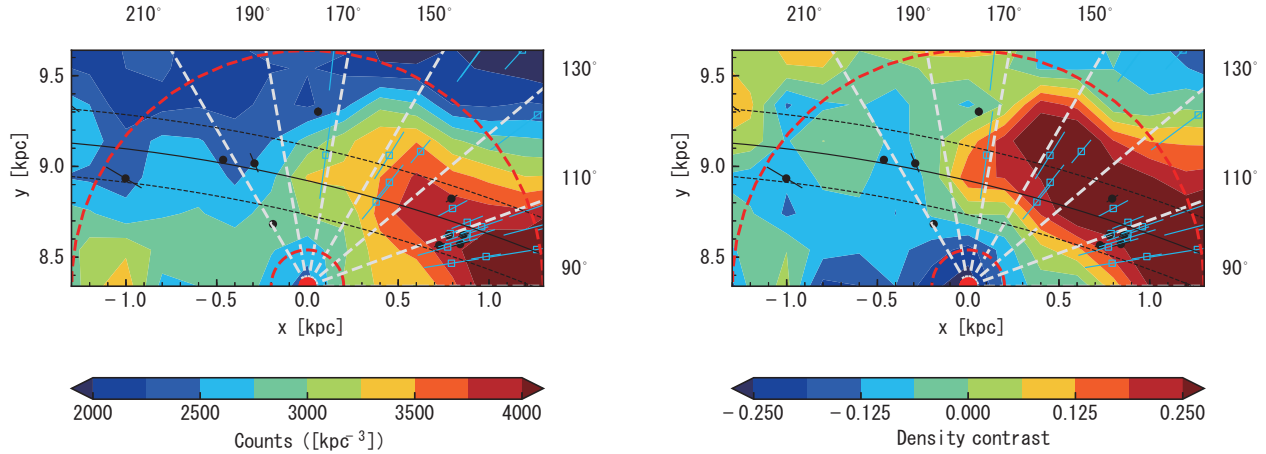


Fig. 3. Miyachi et al. (2019): The smoothed density distribution of 1 Gyr stellar populations (*Left*) and the distribution after divided by an exponential profile with the scale length  $r_d = 2.5$  kpc (e.g., Bland-Hawthorn & Gerhard 2016) (*Right*). The Sun is located at  $(x, y) = (0, 8.34)$  kpc.  $x$ -axis is the direction of the Galactic rotation, and  $y$ -axis is the direction from the Galactic center to the Sun. The location of the Local arm defined with high-mass star forming regions (HMSFRs) is highlighted by the solid black line and the black dashed lines indicate width of the arm (i.e.  $1\sigma$  width). The inner and outer red dashed lines correspond to the distances from the Sun  $d_{xy} = 0.2$  and 1.3 kpc, and we consider that the completeness of our sample is reasonably high in the area between these lines. Filled black circles with error bars show the location of HMSFRs. Open blue squares with error bars indicate the locations of  $H_{II}$  regions in  $90^\circ \leq l \leq 190^\circ$  from Foster & Brunt (2015).

The spatial offset between stellar and gas arms can be explained by the density-wave theory (e.g., see Figure 2 in Dobbs & Pringle 2010). However, the larger pitch angle of the stellar arm compared to the gas arm cannot be explained by the theory. The spatial distribution of star and gas indicates a new and complex picture of the Local arm.

#### REFERENCES

Bland-Hawthorn, J., & Gerhard, O. 2016, *ARA&A*, 54, 529  
 Dobbs, C., & Baba, J. 2014, *PASA*, 31, 35  
 Dobbs, C. L., & Pringle, J. E. 2010, *MNRAS*, 409, 396

Foster, T., & Brunt, C. M. 2015, *AJ*, 150, 147  
 Gaia Collaboration et al. 2018, *A&A*, 616, A1  
 Lindegren, L., Hernandez, J., Bombrun, A., et al. 2018, *A&A*, 616, A2  
 Miyachi, Y., Sakai, N., Kawata, D., et al. 2019, *ApJ*, 882, 48  
 Reid, M. J., Menten, K. M., Brunthaler, A., et al. 2014, *ApJ*, 783, 130  
 Roberts, Jr., W. W. 1972, *ApJ*, 173, 259  
 Sakai, N., Reid, M. J., Menten, K. M., Brunthaler, A., & Dame, T. M. 2019, *ApJ*, 876, 30  
 Sanna, A., Reid, M. J., Dame, T. M., Menten, K. M., & Brunthaler, A. 2017, *Science*, 358, 227  
 Xu, Y., Bian, S. B., Reid, M. J., et al. 2018, *A&A*, 616, L15